Computational and Structural Biotechnology Journal 23 (2024) 1201–1213

Contents lists available at ScienceDirect

Computational and Structural Biotechnology Journal

journal homepage: www.elsevier.com/locate/csbj

Research article

Multi-omics analysis reveals the unique landscape of DLD in the breast cancer tumor microenvironment and its implications for immune-related prognosis

Lijun Xu [a], Lei Yang [b], Dan Zhang [a], Yunxi Wu [a], Jiali Shan [a], Huixia Zhu [c], Zhengyi Lian [a], Guying He [a], Chongyu Wang [d], Qingqing Wang [a,*]

[a] Department of General Surgery, Affiliated Hospital of Nantong University, Medical School of Nantong University, Nantong, China
[b] Department of Clinical Biobank & Institute of Oncology, Affiliated Hospital of Nantong University & Medical School of Nantong University, Nantong, China
[c] Department of Biochemistry, Medical College, Nantong University, Nantong, China
[d] Department of Medicine, Xinglin College, Nantong University, Nantong, China

ARTICLE INFO

Keywords:
Cuproptosis
Breast cancer
Tumor immune microenvironment
Prognostic model

ABSTRACT

Background: Cuproptosis, i.e., copper-induced programmed cell death, has potential implications in cancer therapy. However, the impact of the cuproptosis-related gene (CRG) dihydrolipoyl dehydrogenase (DLD) on breast cancer (BC) prognosis remains underexplored.

Methods: We employed real-time quantitative PCR and multiplexed immunostaining techniques to quantify DLD expression in both BC and the adjacent non-cancerous tissues. Immunofluorescence analysis was employed to assess the influence of DLD on immune cells and immunological checkpoints in the BC microenvironment. DLD knockdown experiments were conducted in BC cell lines MDA-MB-468 and SK-BR-3, with knockdown efficiency validated via western blot. Subsequently, we performed the cell counting kit-8 (CCK-8) assay, clone formation assay, Transwell migration assay, and invasion assay. To construct a prognostic model, we employed a Lasso-Cox regression analysis of immune-related genes associated with DLD. Additionally, we established a competing endogenous RNA network based on CRGs to evaluate potential regulatory pathways.

Results: Compared to the adjacent tissues, BC tissues exhibited markedly elevated DLD expression levels. In vitro experiments demonstrated that DLD knockdown effectively inhibited BC cell migration, invasion, and proliferation. DLD exhibited positive correlations with $CD68^+$ macrophages and PD-L1 in the tumor, as well as with macrophages and $CD4^+$ T cells in the stroma. Tumor regions with high DLD expression were enriched in PD-L1 and macrophages, while stromal regions with high DLD expression contained $CD4^+$ T cells and macrophages. The AUC values for 1-, 3-, and 5-year overall survival in TCGA-BRCA training set were 0.67, 0.66, and 0.66, respectively. A nomogram with a C-index of 0.715 indicated that risk score, tumor stage, and age could serve as independent prognostic factors for BC.

Conclusion: Our findings underscore the significant predictive significance of DLD in BC and its influence on the tumor microenvironment. DLD represents a promising diagnostic and prognostic marker for BC, offering novel avenues for the identification of therapeutic targets and the enhancement of immunotherapy in BC.

1. Introduction

Lung cancer was once the most prevalent malignant tumor worldwide; however, it has now been surpassed in incidence by female breast cancer (BC) [1]. In the United States, the 5-year survival rate for early-stage BC is 90%, but it significantly drops to 29% once distant metastases occur[2]. Currently, treatment options for female patients with BC include surgery, radiation, chemotherapy, endocrine therapy, and targeted treatments [3–6]. Although these treatments improve patient survival, they can also result in long-term effects that considerably impact survivors' quality of life. For example, surgery may cause physical trauma and have psychological repercussions for patients [7,8]. Radiation therapy and chemotherapy can harm healthy tissues and cells, accelerating cell senescence and increasing the risk of heart disease [9,

* Corresponding author.
E-mail address: wang2qing@sina.com (Q. Wang).

https://doi.org/10.1016/j.csbj.2024.02.016
Received 13 October 2023; Received in revised form 2 February 2024; Accepted 20 February 2024
Available online 6 March 2024

10]. Furthermore, hormone and targeted therapies are effective only for specific subgroups of patients with hormone-responsive or target-sensitive tumors [11]. Therefore, identifying novel diagnostic and therapeutic targets, as well as prognostic biomarkers, has become the foremost priority in combating female BC.

Tumor cells employ various immune evasion mechanisms to establish a tumor immune microenvironment (TIME) that facilitates their proliferation [12]. This microenvironment consists of diverse tumor-infiltrating immune cells (TIICs) possessing both adaptive and innate immune functions, which can have both pro-tumorigenic and anti-tumor effects [13]. Macrophages, for instance, regulate IL-35 through the macrophage-stimulating 1 receptor signaling pathway, thereby promoting BC growth and progression [14]. Neutrophils can either promote cancer progression by enhancing tumor angiogenesis or mediate antibody-dependent cellular cytotoxicity against cancer cells, thus functioning as a double-edged sword [15]. Research suggests that certain subsets of TIICs, such as tumor-infiltrating lymphocytes, hold promise as potential prognostic markers for BC due to considerable lymphocytic infiltration [16]. A promising approach to improving the prognosis of patients with BC involves targeting immune checkpoints (ICPs) PD-L1 and CTLA-4 on T-cell surfaces, which impede tumor growth [17,18]. However, TIME exhibits heterogeneity throughout tumor development. Therefore, a thorough investigation of immune-related prognostic markers in the TIME is necessary to gain a deeper understanding of tumor progression. Currently, there is a lack of comprehensive analysis of immune cell subtypes and checkpoints in the TIME at the tissue level in BC.

Cuproptosis represents a novel manifestation of copper-induced programmed cell death [19]. Copper ions induce cell death by interacting with lipoylated proteins in the tricarboxylic acid (TCA) cycle during mitochondrial respiration [19]. Furthermore, copper ions influence PD-L1 expression, thereby facilitating immune evasion in cancer [20]. Cuproptosis has introduced a promising avenue for the treatment of malignant tumors. Traditionally, cancer cells were believed to favor aerobic glycolysis over the TCA cycle (known as the Warburg effect) as a rapid means of generating energy to fuel tumor progression [21]. However, recent evidence highlights the significant role of the TCA cycle in cancer prognosis. For instance, the activation of the pyruvate dehydrogenase complex through PDHA phosphorylation promotes the TCA cycle, enabling cancer cells to adapt to the metastatic microenvironment and facilitate metastasis [22]. In addition, cuproptosis may be associated with the tumor microenvironment. Numerous current risk models based on cuproptosis-related genes indicate that individuals at high risk exhibit reduced immune cell infiltration [23–25]. However, these findings require further experimental validation.

Dihydrolipoyl dehydrogenase (DLD), a constituent of the pyruvate dehydrogenase complex, regulates cuproptosis through the lipoic acid pathway [19]. This enzyme catalyzes the oxidative conversion of pyruvate into acetyl-CoA [26], an irreversible reaction that provides a cofactor for the TCA cycle, thereby bridging glycolysis and the TCA cycle. A recent study showed that the downregulation of DLD can prevent the growth and metastasis of melanoma [27]. However, the impact of DLD on the biological functions of BC cells and the tumor microenvironment remains unexplored.

To address this knowledge gap, we performed an in-depth analysis of DLD expression at both the mRNA and protein levels. The influence of DLD on BC migration, invasion, and proliferation was assessed by knocking down DLD in various BC cell lines. Immunofluorescence techniques were employed to investigate the relationship between DLD and immune-infiltrating cells, as well as ICPs in the tumor microenvironment. Furthermore, we developed a predictive model to evaluate BC prognosis based on immune-related genes associated with DLD. Our study underscores the potential of DLD as a novel diagnostic and prognostic marker for BC.

2. Materials and methods

2.1. Validation of DLD mRNA expression in BC via reverse real-time quantitative PCR (qPCR)

Twelve pairs of matched BC and adjacent tissues were collected at the Affiliated Hospital of Nantong University. For RNA extraction, 500 μL of RNeasy isolation reagent (Vazyme, Nanjing, China) was added to 25 mg of tissue. Subsequently, the supernatant was mixed with an equal volume of isopropanol and centrifuged to obtain the mRNA precipitate. The resulting RNA pellet was then dissolved in RNase-free ddH_2O. The extracted RNA was reverse transcribed to generate complementary DNA, and qPCR was employed to discern differences in DLD expression between tumor and normal tissues. Each group of samples was subjected to three independent experiments. The relative expression level of DLD was determined using the $2^{-\Delta\Delta CT}$ method. The DLD primers utilized were as follows: (forward) 5′ GAAATGTCCGAAGTTCGCTTGA 3′ and (reverse) 3′ TCAGCTTTCGTAGCAGTGACT 5′. The relative expression was normalized to that of glyceraldehyde-3-phosphate dehydrogenase (GAPDH) using the following primers: (forward) 5′ AACGGATTTGGTCGTATTGGG 3′ and (reverse) 3′ CCTGGAAGATGGTGATGGGAT 5′.

2.2. Cell culture and reagents

The triple-negative BC cell line MDA-MB-468, the HER-2-positive BC cell line SK-BR-3, and the HEK293T tool cell line were generously provided by the Department of Clinical Biobank at the Affiliated Hospital of Nantong University. We employed Dulbecco's Modified Eagle's Medium (DMEM; Invitrogen, USA) and McCoy's 5 A medium (Procell, China) in our experiments. These media were supplemented with 10% fetal bovine serum (Lonsera, USA) and 1% penicillin/streptomycin (NCM Biotech, China). DMEM was utilized for the cultivation of the MDA-MB-468 and HEK293T cell lines, while McCoy's 5 A medium was employed for the cultivation of the SK-BR-3 cell line.

2.3. Virus packaging and infection

The knockdown sequences for two destination plasmids, DLD-sh1 and DLD-sh2 (Genechem, China), were as follows: GCAGTTGAAAGAAGAGGGTAT and GCTGGGAGAAATGGGTAAATGAA. Packaging plasmids (psPAX2 and pMD2. G) were introduced in a 4:2:5 ratio to the destination plasmid. Subsequently, PEI 40 K (Servicebio, China) was added, and supernatants were collected after 48 and 72 h. Infection was performed during a period of heightened activity in BC cells, and infection efficiency was assessed at the 72-h time point using fluorescence. Stable cell lines exhibiting DLD knockdown were subsequently selected through the application of puromycin.

2.4. Cellular protein extraction and western blot

When the density of cells with DLD knockdown reached 80–90% within the field of view, RIPA lysates (WB3100, NCM Biotech) supplemented with phosphatase inhibitors and protease inhibitors (Epizyme, China) were added to extract proteins. Subsequently, electrophoresis was conducted followed by specific antibody blotting on a membrane. Luminescence signals were detected using a fully automated chemiluminescence image analysis system (4600, Tanon, China).

2.5. Clone formation assay

The requisite volume of cell suspension was added to a 6-well plate. The culture was monitored at 3-day intervals and terminated once clones became discernible in the 6-well plate. Subsequently, cells were fixed with 4% paraformaldehyde for 15 min and stained with 1% crystal violet for an additional 15 min. Next, the staining solution was gently

washed away with running water, and the cells were allowed to air dry.

2.6. CCK-8 assay

An appropriate volume of a suspension of cells validated for DLD knockdown was dispensed into a 96-well plate at a density of 2000 cells/well. Subsequently, 100 μL of 10 × diluted CCK-8 reagent was introduced at 0, 24, 48, 72, and 96 h, respectively. Following a 2-h incubation period, absorbance was measured at OD450 employing a microplate reader (Thermo Fisher Scientific, USA).

2.7. Cell migration and invasion assay

500uL of medium to 24-well plate chambers and 200 μL of pure medium containing 80,000 cells into the smaller chambers (353097, Corning, USA). After a 24-h incubation period, the migrating cells were fixed and stained. For the invasion assay, 10 μL of a high-concentration hydrogel (TEG003, TheWell Bioscience, USA) and 40 μL of a dilution solution (MS01–50, TheWell Bioscience) were added to the chambers, following which the subsequent steps mirrored those of the migration experiments. Observations were conducted using a microscope at a magnification of 200 × , and the analysis encompassed three independent replicates.

2.8. Development and validation of a BC predictive model based on DLD-related immunological genes (DRIGs)

We identified immune-related genes associated with DLD ($P < 0.05$) in the TISID database (http://cis.hku.hk/TISIDB/). BC cases with missing clinical information were excluded from TCGA database. Subsequently, TCGA-BRCA dataset was randomly divided into internal training (n = 754) and validation (n = 321) sets. A Lasso-Cox analysis was performed, and a prognostic model was constructed using the "glmnet" package in R. The DRIG score (DRIGS) was computed as follows: DRIGS = βExp1 + βExp2 + … + βExpN, where "Exp" represents gene expression, "β" signifies the regression coefficient, and "N" denotes the number of genes included in the model. Patients in the training set were categorized into high- and low-DRIGS groups based on a critical value determined using the "maxstat" package in R. Model performance was assessed by generating a receiver operating characteristic curve (ROC) using the "timeROC" package in R. Furthermore, we integrated the model with clinical and pathological data using the "rms" package in R to construct a nomogram and determine its calibration.

2.9. Establishment of a competing endogenous RNA (ceRNA) network based on CRGs

We screened the top 10 mRNAs with the highest correlation to cuproptosis, as reported in published literature [20]. Subsequently, we identified miRNAs associated with these mRNAs using the miRBase database (https://www.mirbase.org/). Based on the identified miRNAs, we explored the associated mRNA, lncRNA, and circRNA profiles using the ENCORI database (https://starbase.sysu.edu.cn/). Subsequently, we constructed a ceRNA network and visualized it using Cytoscape software (v. 3.7.2).

2.10. Detection of DLD expression in BC via multiplexed immunohistochemistry

Breast tissue was paraffin-embedded for fixation. Subsequently, 5-μm-thick sections were generated using a microtome. These sections were subsequently affixed to tissue microarray (TMA) slides and dehydrated and dewaxed via treatment with ethanol and formalin. To facilitate antigen retrieval, we subjected the slides to microwave heating in a 10 × Tris-EDTA buffer solution (pH 9). The slides were then incubated with primary antibodies. Signal amplification was achieved through a fluorophore covalently linked to the tissue, achieved via a secondary antibody conjugated with horseradish peroxidase. This staining process was repeated, and the sections were counterstained with DAPI. The following antibodies were employed: anti-*DLD* (1:4000; ab133551, Abcam, USA), anti-cytokeratin (CK, 1:4000; orb69073, Biorbyt Ltd., UK), anti-CD3 (1:1000; 85061 s, Cell Signaling Technology, USA), anti-CD4 (1:100; ab133616, Abcam), anti-CD8a (1:1000; 85336 s, Cell Signaling Technology), anti-CD66b (1:4000; arg66287, Arigo Biolaboratories Corp., China), anti-CD20 (1:300; ab78237, Abcam), anti-CD68 (1:10000; 76437 s, Cell Signaling Technology), anti-PD-1 (1:100; 13684 T, Cell Signaling Technology), anti-PD-L1 (1:100, 18616 s, Cell Signaling Technology), anti-CTLA-4 (1:500; orb527271, Biorbyt Ltd.), and anti-LAMP3 antibodies (1:500; ab111090, Abcam). All TMA slides were scanned using the Vectra Quantitative Pathology Imaging System (v. 3.0; PerkinElmer Inc.). The percentage of cells displaying positive staining was quantified using the Inform image analysis software (v. 2.6.0; PerkinElmer Inc.). Cell segmentation software was trained based on cytokeratin and DAPI signals. Positive staining thresholds for TIICs and ICP markers were established, allowing the differentiation between areas with positive and negative staining. Subsequently, the cell percentage (ranging from 0% to 100%) of the positive staining areas was calculated. Senior pathologists validated all pathological diagnoses.

2.11. Study population

We obtained BC tissues (n = 122) and adjacent non-cancer tissues (n = 88) from the Affiliated Hospital of Nantong University between 2005 and 2010 for multiplex immunohistochemistry. In 2022, an additional 12 pairs of matched cancer and adjacent non-cancer tissues were obtained for qPCR. Informed consent was obtained for all patients for the secondary use of their tissue samples, and the study was conducted in strict adherence to the ethical guidelines outlined in the Declaration of Helsinki. Patients provided written informed consent prior to the initial sample collection. The ethics committee at the Affiliated Hospital of Nantong University approved the utilization of human tissue samples (approval number: 2021-L001).

2.12. Statistical analysis

The correlation between DLD expression and clinicopathological data was assessed using Pearson's chi-square test. Differences in DLD expression between cancer and adjacent non-cancer tissues were evaluated using the Wilcoxon signed-rank test. Spearman rank correlation analysis was employed to estimate the correlation between DLD and TIICs. The variation in TIIC and ICP infiltration across groups with different DLD expression levels was analyzed using the Wilcoxon signed-rank test. Statistical significance was considered at $P < 0.05$. All data analyses were performed using IBM SPSS Statistics for Windows (v. 26.0; IBM Corp., Armonk, NY, USA) and R software (v. 4.1.2).

3. Results

3.1. DLD is a potential diagnostic and prognostic marker for BC

Analysis of TCGA and GTEx databases revealed that DLD expression was significantly upregulated in BC compared to normal tissue (Fig. 1A). Furthermore, DLD exhibited differential expression across various immune and molecular subtypes of human cancers (Supplementary Figure 1). Analysis of TCGA-BRCA (Fig. 1B), ICGC-BRCA (Fig. 1C), and GSE9893 (Fig. 1D) datasets consistently suggested a poor prognosis associated with elevated DLD expression. Pan-cancer analysis further underscored DLD as a prevalent tumor marker (Supplementary Figure 2). Moreover, DLD expression displayed negative correlations with the estimate score (r = −0.11; P = 1.7e-4) and immune score (r = 0.14; P = 2.5e-6) (Fig. 1E), suggesting its potential in modulating the

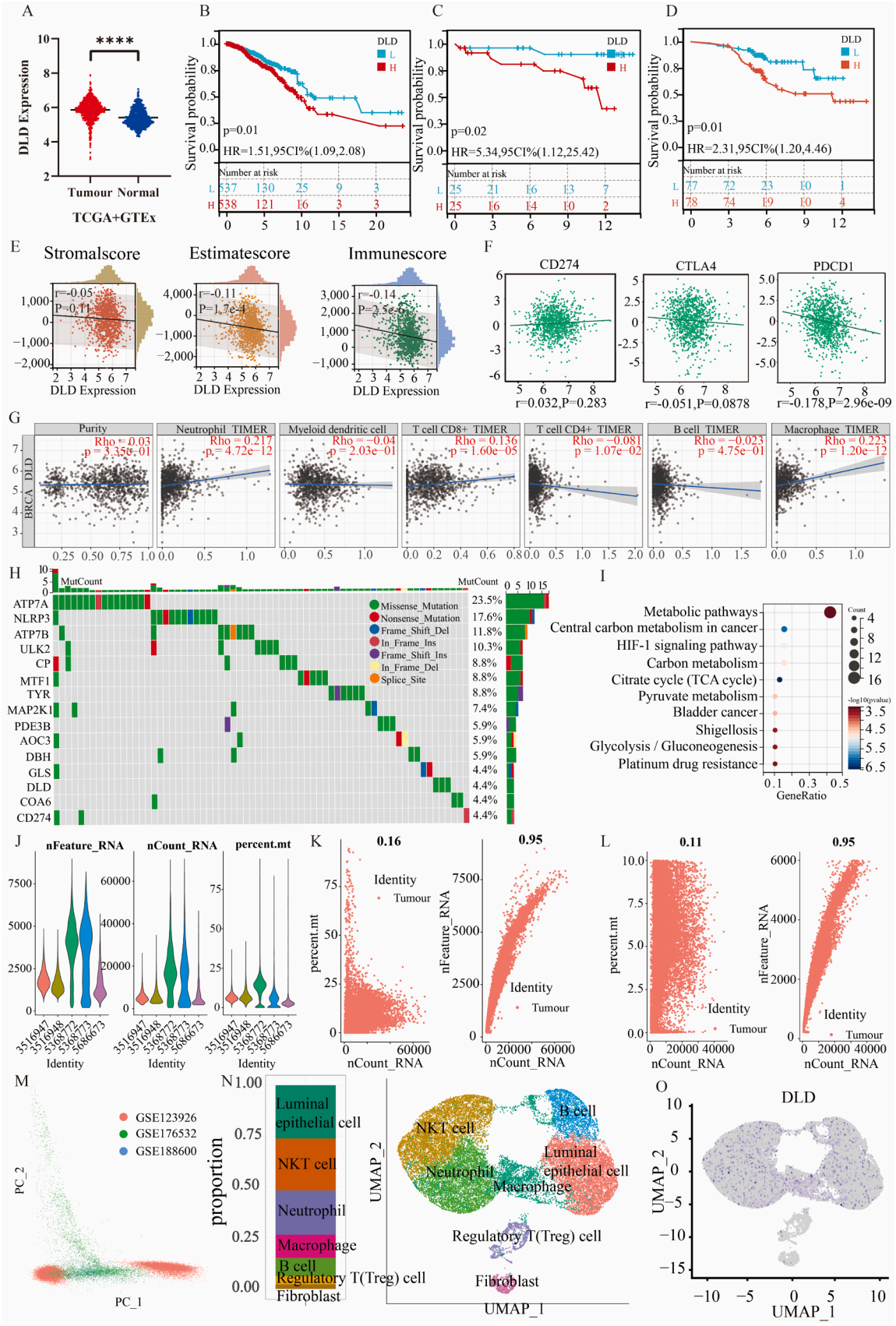

(caption on next page)

Fig. 1. Correlation of DLD expression with BC prognosis and tumor microenvironment. (A) A satterplot illustrating DLD expression in BC and normal tissues. Kaplan–Meier survival curves depicting OS in patients stratified based on DLD expression in (B) TCGA-BRCA, (C) ICGC-BRCA, and (D) GSE9893 datasets. (E) Correlation analysis of DLD expression and stromal, estimate, and immune scores. (F) Correlation analysis of DLD expression and ICPs. (G) Correlation analysis of DLD expression and TIICs based on the TIMER database. (H) Mutation analysis of 49 CRGs. (I) KEGG enrichment analysis of the 49 CRGs. (J) Data pertaining to the quantity of molecules, genes, and mitochondrial genome copies in each cell, along with the percentage of each cell's mitochondrial genome. The x-axis represents various sample values, whereas the y-axis displays the number of genes discovered or mitochondrial content. The left graph depicts the relationship between the total number of molecules in the cell before (K) and after (L) data filtering, as well as mitochondrial content. (M) A graph of principal component analysis (PCA) following the removal of batch effects. The vertical coordinates denote the proportion of each cell, whereas the horizontal coordinates represent distinct groups. (N) The distribution of various cell proportions and cell distribution maps. (O) Differential expression of DLD across diverse cell types.

TIME. Subsequently, we investigated the relationship between DLD and ICPs. DLD demonstrated a negative correlation with PD-1 ($r = -0.178$; $P = 2.96e\text{-}9$) (Fig. 1F). Subsequently, we investigated the TIMER database, which revealed associations between DLD and various immune infiltrating cells (Fig. 1G), including neutrophils ($r = 0.217$; $P < 0.001$), $CD4^+$ T cells ($r = -0081$; $P = 0.0107$), $CD8^+$ T cells ($r = 0.22$; $P = 9.7E\text{-}14$), and macrophages ($r = 0.28$; $P = 2.6e\text{-}21$). Analysis of the mutations in 49 CRGs [19,28–30] in 985 TCGA-BRCA samples revealed genetic variations in 57 (5.8%) samples, with ATP7A and NLRP3 being the predominant mutated genes (Fig. 1H). KEGG pathway enrichment analysis of these 49 CRGs revealed that they were primarily enriched in carbon metabolic and hypoxia-inducible factor (HIF-1) signaling pathways (Fig. 1I). We performed quality control assessments, examining gene information, the total number of molecules, and the percentage of mitochondrial genomes in cells from GSE123926, GSE176532, and GSE188600 (Fig. 1J–L). Prior to principal component analysis, we pooled 2000 high-frequency genes to mitigate batch effects, followed by screening through canonical correlation analysis (Fig. 1M). This process enabled the identification of seven distinct cell types, including B cells, neutrophils, macrophages, natural killer (NK) T cells, regulatory T cells,

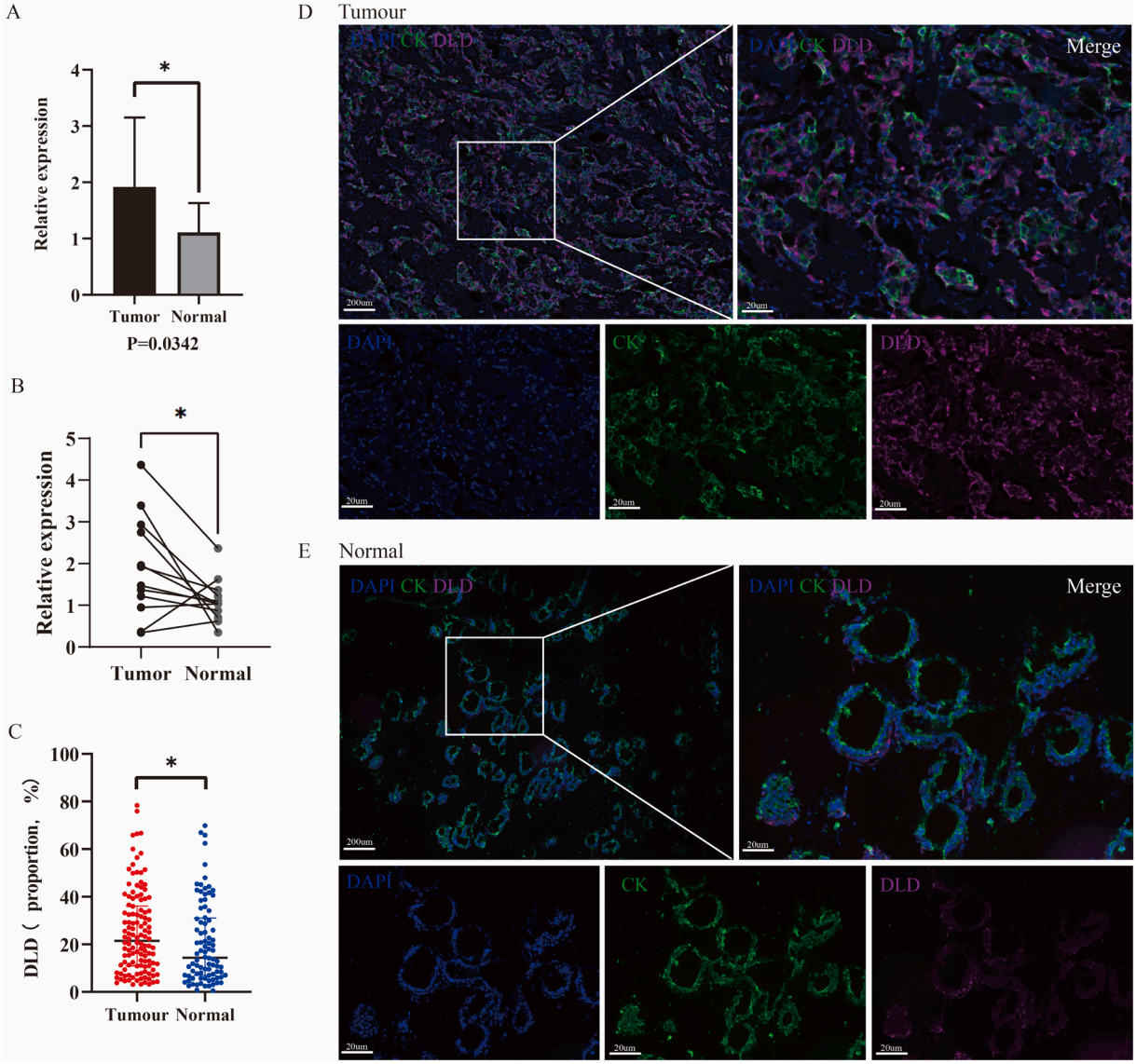

Fig. 2. Differential expression of DLD between BC and adjacent tissues. (A, B) Evaluation of the differential mRNA expression of DLD between BC and adjacent tissues via qPCR. (C) A scatterplot depicting the protein expression of DLD in BC and adjacent tissues (D, E) mIHC validation of the differential protein expression of DLD between BC and adjacent tissues.

fibroblasts, and breast epithelial cells, based on cell-specific markers. Within the BC tumor microenvironment, DLD exhibited differential expression patterns (Fig. 1N, O). Additionally, we observed a significant correlation between DLD expression and TIME, immunotherapy biomarkers, and ICPs across a spectrum of cancer types (Supplementary Figures 3, 4).

3.2. Expression of DLD is higher in BC tissues compared to normal tissues

We investigated DLD expression in 12 pairs of matched BC and adjacent non-cancerous tissues via qPCR. Our analysis revealed a marked increase in DLD expression in BC tissues (n = 122) compared to non-cancerous tissues (n = 88; $P = 0.0342$) (Fig. 2A, B). This finding was further corroborated by multiplexed immunohistochemistry, which revealed elevated levels of the protein expression of DLD in BC tissues (Fig. 2C–E).

3.3. Correlation between DLD protein expression, BC prognosis, and clinicopathological features

We assessed the correlation between the protein expression of DLD and clinicopathological features of patients with BC using the Pearson product-moment correlation coefficient. DLD expression exhibited associations with age (Pearson $\chi2 = 5.299$; $P = 0.022$), T (Pearson $\chi2 = 14.705$; $P = 0.002$), and N (Pearson $\chi2 = 10.058$; $P = 0.018$; Table 1). Furthermore, both univariate and multivariate Cox regression analyses indicated that DLD expression ($P = 0.001$), N category ($P < 0.0001$), and HER-2 status ($P = 0.029$) were independent prognostic factors for unfavorable overall survival (OS) outcomes among the patients (Table 2).

3.4. Correlation among the protein expression of DLD, TIICs, and ICPs in BC TIME

We employed multiplexed immunohistochemistry-derived expression data to examine the association between DLD and TIICs as well as ICPs in the TIME of BC. Spearman rank correlation analysis revealed distinct immune infiltration patterns between the tumor and interstitial regions of BC. In the tumor region, DLD expression exhibited a positive correlation with $CD68^+$ macrophages and PD-L1 (Fig. 3A). Additionally, in the stromal region, a positive correlation was observed between DLD expression and the presence of macrophages and $CD4^+$ T cells (Fig. 3B). In addition, tumor regions with high DLD expression demonstrated an enrichment of macrophages and PD-L1 (Fig. 3C), while stromal regions with elevated DLD expression exhibited an increased presence of $CD4^+$ T cells and macrophages (Fig. 3D). To visualize the spatial distribution of ICPs and TIICs, we employed the Vectra Quantitative Pathology Imaging System (Fig. 3E–G).

3.5. Development and validation of a prognostic model based on DRIGS

We identified 18 immune-related genes associated with DLD in the TISID database ($P < 0.05$; Fig. 4A). These genes were utilized to construct a prognostic model through Lasso-Cox regression analysis. The following formula was employed: DRIGS $= 0.067175 \times$ CD276 - $0.103028 \times$ TNFRSF14 $+ 0.05778 \times$ ULBP1 (Fig. 4B). Each patient's prognostic information was represented as a prognostic curve and scatterplot. The thermogram displaying the expression profiles of the candidate DRIGs revealed that TNFRSF14 expression was lower in the high-DRIGS group, while CD276 and ULBP1 expression were higher (Fig. 4C, D). In comparison, the OS of patients in the high-DRIGS group was substantially lower than that in the low-DRIGS group (Fig. 4E, G). ROC analysis demonstrated that the area under curve (AUC) for OS at 1, 3, and 5 years was 0.67, 0.66, and 0.66, respectively (Fig. 4F), and 0.61, 0.70, and 0.71, respectively, in the validation set (Fig. 4H). Moreover, these findings were corroborated by external training sets, namely GSE42568, GSE20685, and GSE88770 (Supplementary Figure 5). Univariate and multivariate Cox analyses indicated that age, risk score, and tumor stage could serve as independent prognostic factors for BC. A nomogram model was subsequently constructed using these independent risk factors (Fig. 4I). The performance of this nomogram was validated employing the C-index (C = 0.715; 95% CI = 0.683–0.747) and a calibration curve (Fig. 4J).

Table 1
Correlation between the protein expression of DLD and clinicopathological characteristics in BC.

Characteristics	High (n = 42)	Low (n = 80)	Total (n = 122)	χ2	P
Age				5.229	**0.022**
> 60	27 (22.13%)	34 (27.87%)	61 (50.00%)		
≤ 60	15 (12.30%)	46 (37.70%)	61 (50.00%)		
ER				2.737	0.434
0	16 (13.11%)	42 (34.43%)	58 (47.54%)		
1	10 (8.20%)	15 (12.30%)	25 (20.49%)		
2	10 (8.20%)	12 (9.84%)	22 (18.03%)		
3	6 (4.92%)	11 (9.02%)	17 (13.93%)		
PR				2.499	0.475
0	28 (22.95%)	53 (43.44%)	81 (66.39%)		
1	1 (0.82%)	7 (5.74%)	8 (6.56%)		
2	7 (5.74%)	13 (10.66%)	20 (16.39%)		
3	6 (4.92%)	7 (5.74%)	13 (10.66%)		
HER-2				5.500	0.139
0	5 (4.10%)	16 (13.11%)	21 (17.21%)		
1	12 (9.84%)	10 (8.20%)	22 (18.03%)		
2	11 (9.02%)	27 (22.13%)	38 (31.15%)		
3	14 (11.48%)	27 (22.13%)	41 (33.61%)		
T				14.705	**0.002**
0	7 (5.74%)	25 (20.49%)	32 (26.23%)		
1	10 (8.20%)	33 (27.05%)	43 (35.25%)		
2	16 (13.11%)	9 (7.38%)	25 (20.49%)		
3	9 (7.38%)	13 (10.66%)	22 (18.03%)		
N				10.058	**0.018**
0	24(19.67%)	23 (18.85%)	47 (38.52%)		
1	14(11.48%)	42 (34.43%)	56 (45.90%)		
2	2 (1.64%)	11 (9.02%)	13 (10.66%)		
3	2 (1.64%)	4 (3.28%)	6 (4.92%)		
M				3.016	0.082
No metastasis	39 (31.97%)	79 (64.75%)	118 (96.72%)		
Metastasis	3 (2.46%)	1 (0.82%)	4 (3.28%)		

ER: estrogen receptor; PR: progesterone receptor; HER-2: human epidermal growth factor receptor-2

3.6. Post-modeling multiplex analysis

Differentially expressed genes (DEGs) were identified between the high- and low-DRIGS groups (Fig. 5A). Subsequently, KEGG enrichment analysis revealed that these groups exhibited enrichment primarily in pathways associated with ferroptosis, human cytomegalovirus infection, and HIF-1 signaling (Fig. 5B). An analysis of immune infiltration, conducted using the CIBERSORT database, demonstrated a higher prevalence of eosinophils, $CD4^+$ T cells, $CD8^+$ T cells, and mast cells in the low-DRIGS group. Conversely, dendritic cells (DCs), macrophages, and

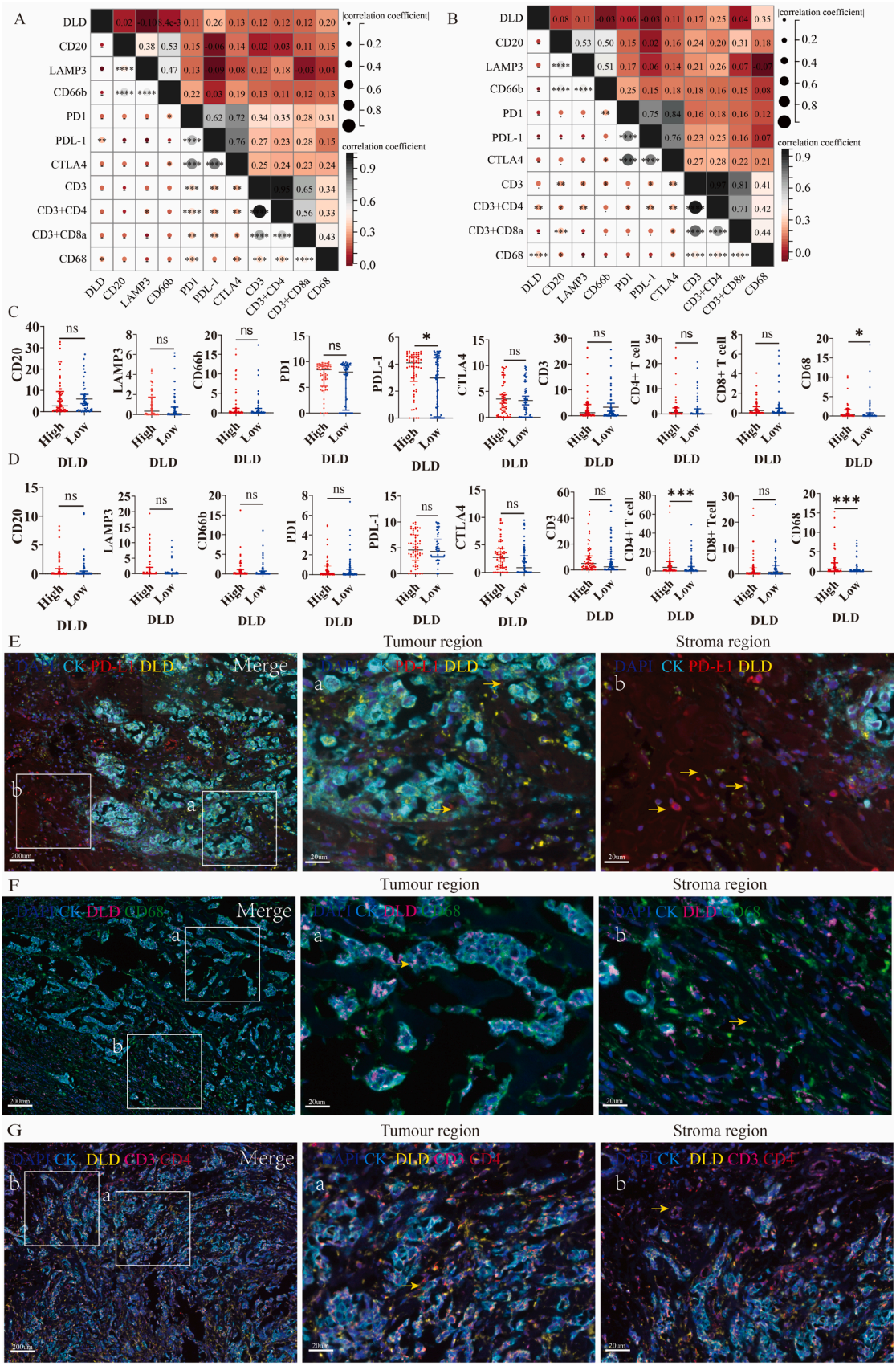

Fig. 3. Evaluation of TIICs and ICPs in BC. Correlation analysis of DLD, TIICs, and ICPs in the tumor (A) and stromal regions (B) of BC. A scatterplot depicting the correlation between DLD expression and various ratios of TIICs and ICPs in the tumor (C) and stromal regions (D) of BC. (E) Four-color multispectral composite images of DAPI, CK, PD-L1, and DLD. (F) Four-color multispectral composite images of DAPI, CK, CD68, and DLD. (G) Five-color multispectral composite images of DAPI, CK, CD3, CD4, and DLD.

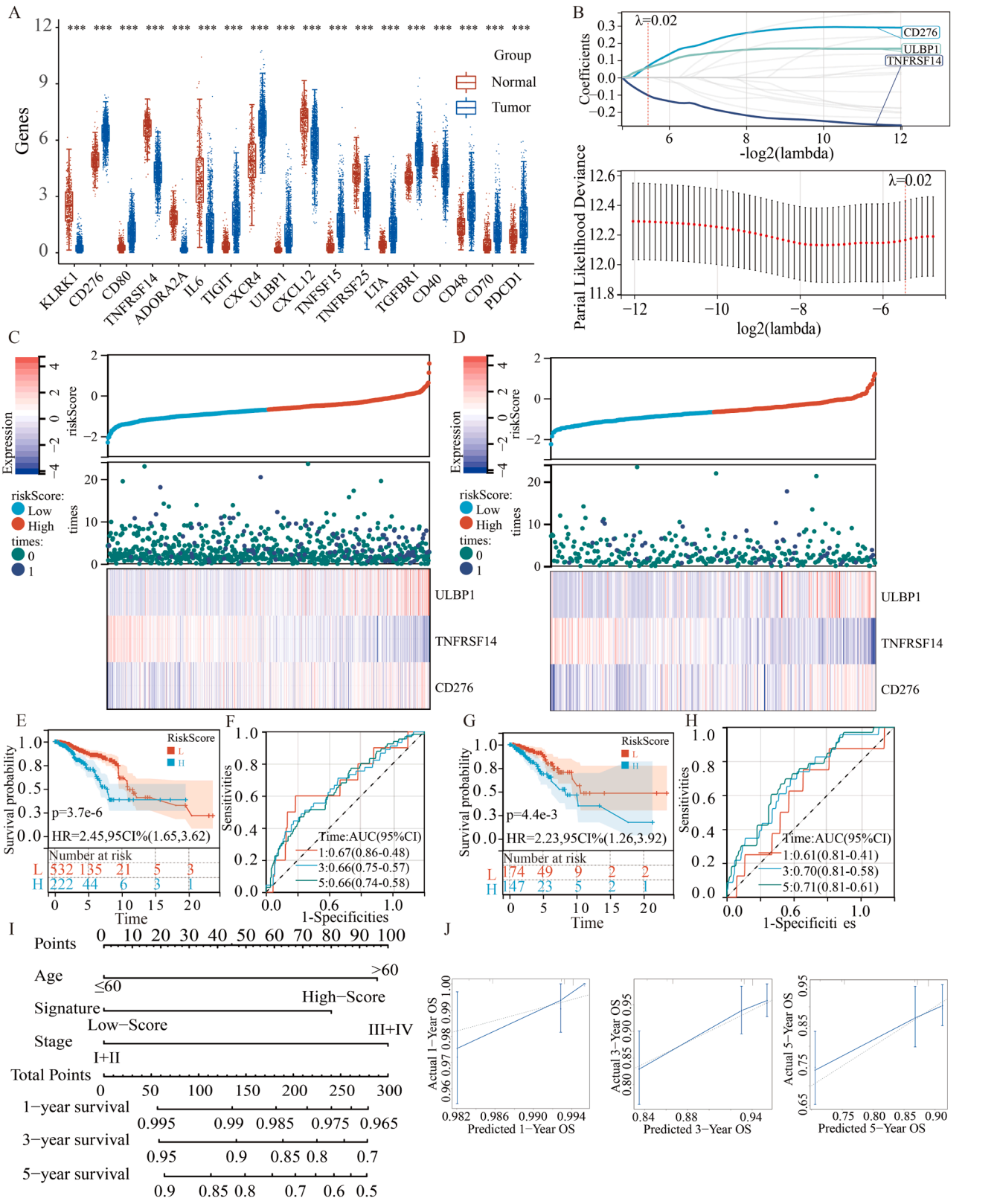

Fig. 4. Development and validation of a prognostic model based on DLD. (A) Differential expression of DRIGs in tumor and normal tissues. (B) Lasso-Cox analysis with a 10-fold cross-validation, evaluating the prognostic value of DRIGS. Distribution of DRIGS and a heatmap of the three-gene model in the training (C) and validation sets. (D) Kaplan–Mayer curve of the three-gene model in the training I and validation sets (G). Time-dependent ROC analysis of the three-gene model for 1-, 3-, and 5-year OS in the training (F) and validation sets (H). (I) A nomogram combining age signature and stage. (J) Calibration analysis of the nomogram for 1-, 3-, and 5-year survival rates.

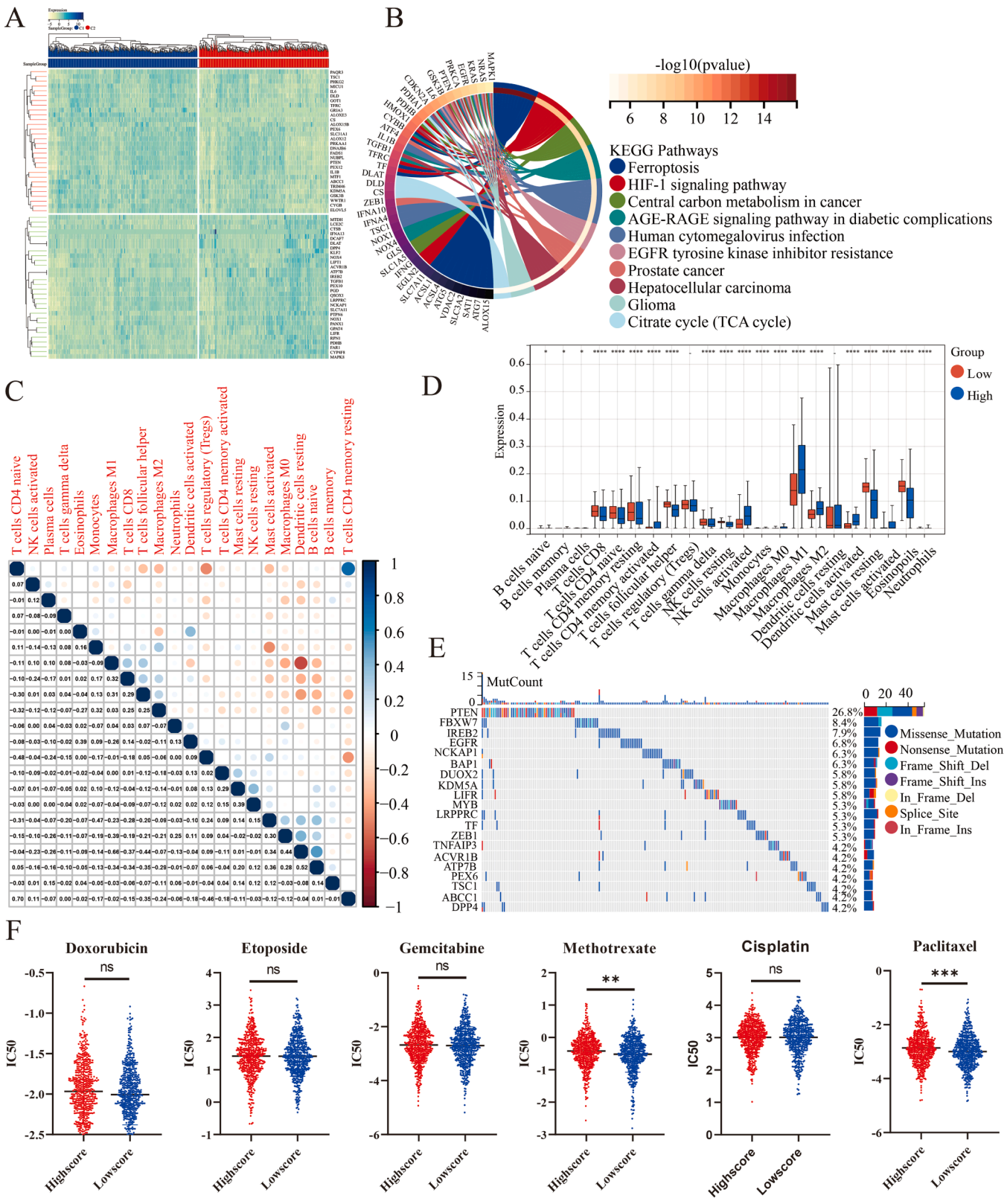

Fig. 5. Post-modeling multiplex analysis. (A) A heatmap of DEGs between high- and low-risk groups. (B) Enrichment analysis of DEGs. (C) Correlation analysis of TIICs based on the DEGs. (D) Differentially expressed TIICs between high- and low-risk groups. (E) Mutation analysis in the high-DRIGS group. (F) Analysis of variations in sensitivity to chemotherapeutic medication between the high- and low-risk groups.

NK cells were more abundant in the high-DRIGS group (Fig. 5C, D). In the high-DRIGS group, PTEN, FBXW7, and IREB2 exhibited the highest mutation frequencies, while in the low-DRIGS group, TP53, PIK3CA, and TTN ranked as the top three mutated genes (Fig. 5E, Supplementary Figure 6). Furthermore, the low-DRIGS group displayed increased sensitivity to methotrexate and paclitaxel, which may signify a more favorable prognosis (Fig. 5F).

3.7. Knockdown of DLD inhibits BC cell proliferation, migration, and invasion in vitro

We validated the efficacy of DLD knockdown in two distinct types of BC cells through western blot analysis (Fig. 6A). Quantification of the bands using ImageJ software further substantiated the significant reduction in the expression of DLD in sh1 and sh2 cells compared to negative control cells (Fig. 6B). Subsequently, Transwell assays revealed a significant reduction in both migration (Fig. 6C) and invasion (Fig. 6D) of BC cells following DLD knockdown. Furthermore, the results of a CCK-8 assay (Fig. 6E) and a clone formation assay (Fig. 6F) indicated that inhibiting DLD diminished the proliferative capacity of BC cells. Collectively, these findings provide evidence that DLD promotes the in vitro progression of BC cells.

3.8. Establishment of co-expression and ceRNA networks based on CRGs

We examined the co-expression network of DLD in BC using the LinkedOmics database. The molecules co-expressed with DLD in BC are visually depicted in a volcano plot (Fig. 7A) and heatmaps (Fig. 7B, C). Subsequently, we conducted an enrichment analysis of the co-expressed genes. GO analysis indicated that the DLD co-expression network was primarily associated with the tRNA metabolic processes and extracellular matrix structural constituents (Fig. 7D–F). Additionally, KEGG analysis revealed that the co-expressed genes were primarily enriched in RNA transport (Fig. 7G). We also constructed a ceRNA network using Cytoscape (v. 3.7.2), which consisted of 10 mRNA nodes associated with cuproptosis, 14 lncRNA nodes, 8 circRNA nodes, and 19 miRNA nodes (Fig. 7H).

4. Discussion

BC stands as the most prevalent malignancy among females globally, and its prognosis varies significantly due to inherent heterogeneity [31]. Identifying novel therapeutic targets is paramount to improving patient prognosis.

In this study, we substantiated elevated DLD expression levels in BC, contrasted with low expression in adjacent non-cancerous tissues, both

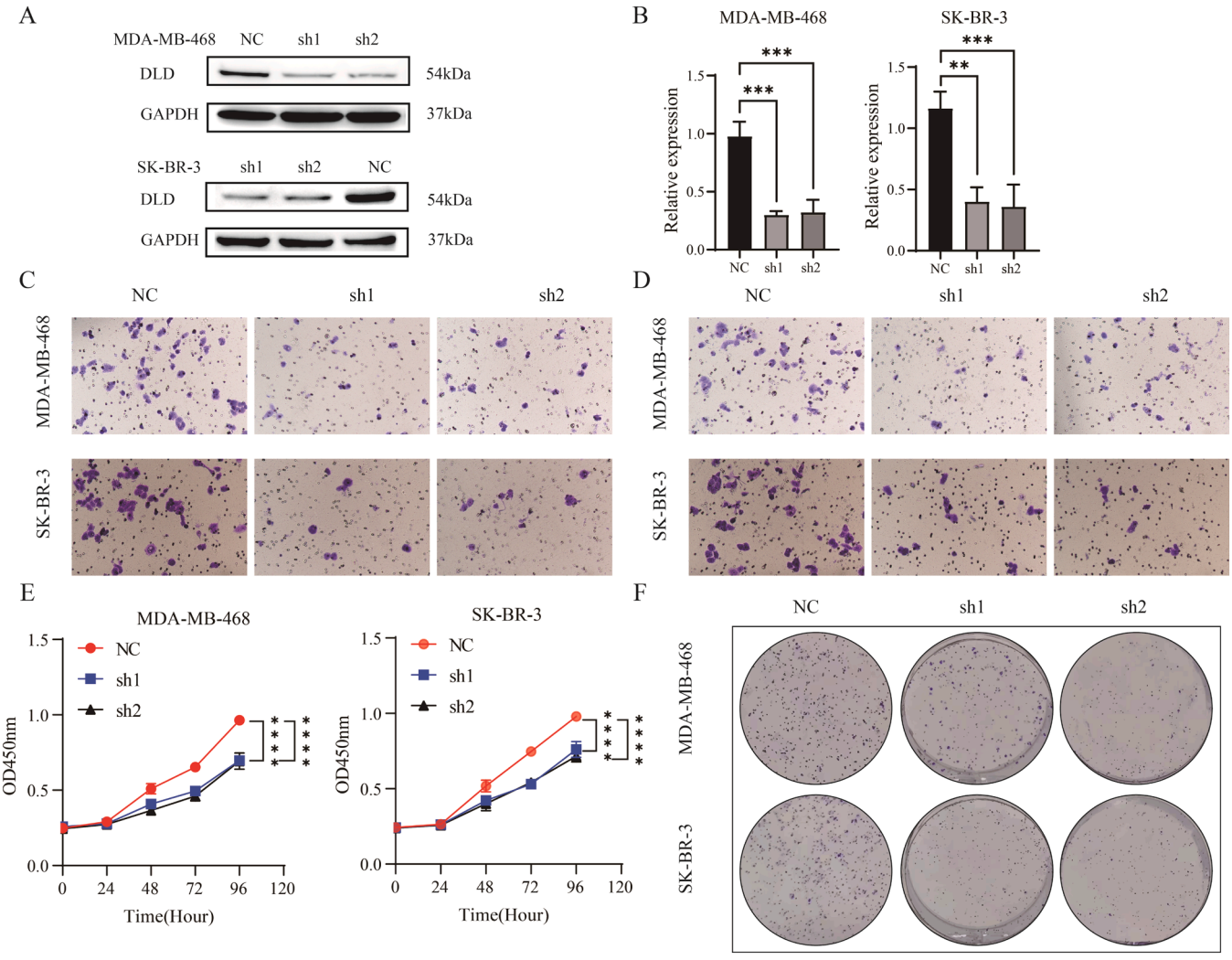

Fig. 6. Knockdown of DLD inhibits BC cell proliferation, migration, and invasion in vitro. (A) Validation of the efficiency of DLD knockdown in BC cells. (B) The relative expression of DLD in each BC cell following DLD knockdown. After quantifying the expression levels of DLD and *GAPDH* using ImageJ software, we calculated the relative expression of DLD. Images of Transwell migration (C) and invasion (D) of BC cells with varying DLD expression levels. (E) Line charts depicting the CCK-8 assay results for BC cells with varying DLD expression levels. (F) Images of colony formation by BC cells with varying DLD expression levels.

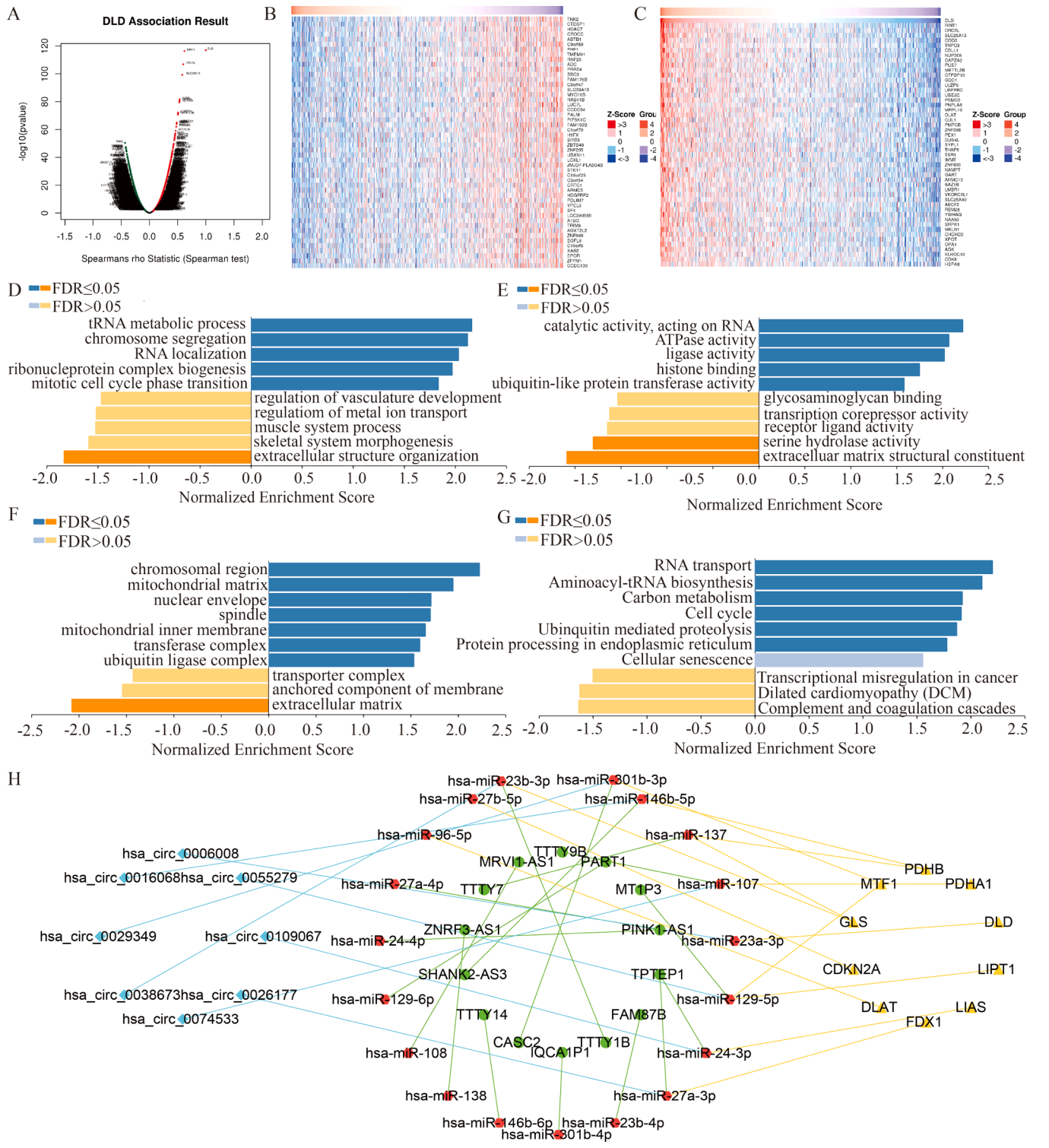

Fig. 7. Establishment of co-expression and ceRNA networks based on CRGs. (A) A volcano map displaying genes highly correlated with DLD expression in the BC cohort. A heatmap of the top 50 co-expressed genes exhibiting a negative correlation (B) or a positive correlation (C) with DLD expression in BC. BP (biological process, D), MF (molecular function, E), CC (cellular component, F), and KEGG (G) enrichment analysis of the co-expression network. (H) Establishment of a ceRNA network based on CRGs.

at the mRNA and protein levels. We validated these findings through qPCR and multiplexed immunohistochemical staining. Furthermore, our investigations revealed a correlation between DLD expression and TNM staging. Moreover, we identified DLD expression, N category, and HER-2 status as independent prognostic factors negatively impacting OS in patients. These findings underscore the clinical significance of DLD as a promising diagnostic target and a valuable prognostic marker for BC.

Current prognostic tumor markers include TIICs and ICPs [32]. In this study, we investigated the role of DLD in the TIME of BC. Our findings revealed a negative correlation between DLD expression and PD-1, a common checkpoint protein found on the surface of T cells known for its immune suppressive properties. Conversely, DLD

exhibited positive correlations with various immune cell populations, including $CD4^+$ T cells, $CD8^+$ T cells, B cells, DCs, macrophages, and neutrophils. Multiplexed immunostaining further demonstrated that DLD expression was positively associated with macrophages and PD-L1 expression in the tumor region of BC, as well as with $CD68^+$ macrophages and $CD4^+$ T cells in the interstitial region. Our experimental findings corroborated data obtained from databases, although some TIICs appeared unrelated to DLD. These findings suggest that increasing the sample size in future studies may provide more precise insights. Combining PD-1 and PD-L1 inhibition has been shown to hinder T cell-mediated cancer cell killing, with the anti-PD-L1 antibody and azithromycin conjugate demonstrating effectiveness against BC cell lines [33,34]. Tumor-associated macrophages are associated with a poor prognosis in most cancer types [35]. These macrophages can be classified into two subtypes: M1, which inhibits tumor growth, and M2, which promotes it [36]. Our results indicated a positive association between DLD and macrophage infiltration in the TIME of BC, indicating that DLD may influence the TIME by interacting with PD-L1 and M2 macrophages, potentially contributing to a poorer prognosis. The positive correlation between DLD expression in the BC stroma and $CD4^+$ T cells aligns with data from the TIMER database. Helper $CD4^+$ T cells have been shown to enhance the anti-tumor response of cytotoxic $CD8^+$ T cells, and recently, $CD4^+$ cytotoxic T cells have been detected in the context of cancer, demonstrating their potential to eliminate tumors such as melanoma [37,38]. Therefore, $CD4^+$ T cells may represent promising therapeutic targets for DLD, influencing the prognosis of BC.

At present, an increasing number of prognostic models focus on tumor immunity. In their research, some scholars have focused on identifying mutated genes that impact the OS of patients with melanoma treated with CTLA-4 inhibitors. These genes were mapped to relevant pathways to construct and validate the model [39,40]. Our investigation revealed an association between DLD and several immune-related genes. Consequently, we constructed a three-gene prognostic model comprising CD276, TNFRSF14, and ULBP1. Previous studies have established that *CD276* promotes the proliferation of BC cells, as evidenced by human BC xenografts in mice [41]. Moreover, the overexpression of TNFRSF14 has been shown to impede the proliferation of MCF-7 BC cells [42]. ULBP1, serving as a ligand for NKG2D, exhibited heightened expression with higher BC tumor grades and a greater prevalence of lymph node-positive tumors [43]. Despite the well-established association of these genes with BC pathogenesis, we are the first to consolidate them as prognostic markers for patients with BC.

Nonetheless, our study has a few limitations. Firstly, we conducted the study with a limited sample size, which could potentially introduce statistical errors. Secondly, we did not explore the mechanisms underlying the immune microenvironment and the biological behavior of DLD in relation to BC through in vivo experiments.

5. Conclusion

Our study represents the first to investigate the impact of DLD expression on both the prognosis and the TIME in patients with BC. DLD is significantly overexpressed in BC tissues, making it a potential diagnostic marker for this condition. Our findings elucidate the intricate associations between DLD expression, the extent of immune cell infiltration, and the expression of ICPs. Consequently, DLD holds promise as a valuable prognostic tool for predicting outcomes in patients with BC, warranting further investigation.

Authors' contributions

LJX conceived the study's concept, conducted the experiments, wrote and revised the manuscript. Picture optimization was overseen by LY and DZ. YXW, GYH, ZYL, and HXZ performed data analysis. The manuscript was comprehensively revised for significant intellectual content by CYW, JLS, and QQW. All authors reviewed and approved the final version of the manuscript.

Funding

This study was supported by grants from the Research Project on Teaching Reform of Nantong University (2020B43), the Jiangsu Province Capability Improvement Project through Science, Technology and Education (ZDXK202234), the Jiangsu Provincial Research Hospital (YJXYY202204), China, Jiangsu Provincial Health Commission Project (X202356), Jiangsu Provincial Research Hospital (YJXYY202204-YSB23), and the Postgraduate Research & Practice Innovation Program of Jiangsu Province (SJCX22_1631).

Declaration of Competing Interest

The authors declare that they have no competing interests.

Appendix A. Supporting information

Supplementary data associated with this article can be found in the online version at doi:10.1016/j.csbj.2024.02.016.

References

[1] Sung H, Ferlay J, Siegel RL, Laversanne M, Soerjomataram I, Jemal A, et al. Global cancer statistics 2020: GLOBOCAN estimates of incidence and mortality worldwide for 36 cancers in 185 countries. CA Cancer J Clin 2021;71(3):209–49.
[2] Giaquinto AN, Sung H, Miller KD, Kramer JL, Newman LA, Minihan A, et al. Breast cancer statistics, 2022. CA Cancer J Clin 2022;72(6):524–41.
[3] Andre F, Ismaila N, Allison KH, Barlow WE, Collyar DE, Damodaran S, et al. Biomarkers for adjuvant endocrine and chemotherapy in early-stage breast cancer: ASCO guideline update. J Clin Oncol 2022;40(16):1816–37.
[4] Burstein HJ, Curigliano G, Thürlimann B, Weber WP, Poortmans P, Regan MM, et al. Customizing local and systemic therapies for women with early breast cancer: the St. Gallen International Consensus Guidelines for treatment of early breast cancer 2021. Ann Oncol 2021;32(10):1216–35.
[5] Cucciniello L, Gerratana L, Del Mastro L, Puglisi F. Tailoring adjuvant endocrine therapy in early breast cancer: When, how, and how long? Cancer Treat Rev 2022; 110:102445.
[6] Waks AG, Winer EP. Breast cancer treatment: a review. JAMA 2019;321(3): 288–300.
[7] Al-Hilli Z, Wilkerson A. Breast surgery: management of postoperative complications following operations for breast cancer. Surg Clin North Am 2021; 101(5):845–63.
[8] Rockson SG. Lymphedema after breast cancer treatment. New Engl J Med 2018; 379(20):1937–44.
[9] Henson KE, McGale P, Darby SC, Parkin M, Wang Y, Taylor CW. Cardiac mortality after radiotherapy, chemotherapy and endocrine therapy for breast cancer: Cohort study of 2 million women from 57 cancer registries in 22 countries. Int J Cancer 2020;147(5):1437–49.
[10] Sehl ME, Carroll JE, Horvath S, Bower JE. The acute effects of adjuvant radiation and chemotherapy on peripheral blood epigenetic age in early stage breast cancer patients. NPJ Breast Cancer 2020;6:23.
[11] Loibl S, Poortmans P, Morrow M, Denkert C, Curigliano G. Breast cancer. Lancet 2021;397(10286):1750–69.
[12] Binnewies M, Roberts EW, Kersten K, Chan V, Fearon DF, Merad M, et al. Understanding the tumor immune microenvironment (TIME) for effective therapy. Nat Med 2018;24(5):541–50.
[13] Fu T, Dai L-J, Wu S-Y, Xiao Y, Ma D, Jiang Y-Z, et al. Spatial architecture of the immune microenvironment orchestrates tumor immunity and therapeutic response. J Hematol Oncol 2021;14(1):98.
[14] Ruiz-Torres SJ, Bourn JR, Benight NM, Hunt BG, Lester C, Waltz SE. Macrophage-mediated RON signaling supports breast cancer growth and progression through modulation of IL-35. Oncogene 2022;41(3):321–33.
[15] Li MO, Wolf N, Raulet DH, Akkari L, Pittet MJ, Rodriguez PC, et al. Innate immune cells in the tumor microenvironment. Cancer Cell 2021;39(6):725–9.
[16] Zhang S-C, Hu Z-Q, Long J-H, Zhu G-M, Wang Y, Jia Y, et al. Clinical Implications of Tumor-Infiltrating Immune Cells in Breast Cancer. J Cancer 2019;10(24): 6175–84.
[17] Krasniqi E, Barchiesi G, Pizzuti L, Mazzotta M, Venuti A, Maugeri-Saccà M, et al. Immunotherapy in HER2-positive breast cancer: state of the art and future perspectives. J Hematol Oncol 2019;12(1):111.
[18] Wang D-R, Wu X-L, Sun Y-L. Therapeutic targets and biomarkers of tumor immunotherapy: response versus non-response. Signal Transduct Target Ther 2022;7(1):331.
[19] Tsvetkov P, Coy S, Petrova B, Dreishpoon M, Verma A, Abdusamad M, et al. Copper induces cell death by targeting lipoylated TCA cycle proteins. Science 2022;375 (6586):1254–61.

[20] Voli F, Valli E, Lerra L, Kimpton K, Saletta F, Giorgi FM, et al. Intratumoral Copper Modulates PD-L1 Expression and Influences Tumor Immune Evasion. Cancer Res 2020;80(19):4129–44.
[21] Icard P, Shulman S, Farhat D, Steyaert J-M, Alifano M, Lincet H. How the Warburg effect supports aggressiveness and drug resistance of cancer cells? Drug Resist Updat 2018:38.
[22] Cai Z, Li C-F, Han F, Liu C, Zhang A, Hsu C-C, et al. Phosphorylation of PDHA by AMPK Drives TCA Cycle to Promote Cancer Metastasis. Mol Cell 2020;80(2).
[23] Chen B, Zhou X, Yang L, Zhou H, Meng M, Zhang L, et al. A Cuproptosis Activation Scoring model predicts neoplasm-immunity interactions and personalized treatments in glioma. Comput Biol Med 2022;148:105924.
[24] Chen Y, Tang L, Huang W, Abisola FH, Zhang Y, Zhang G, et al. Identification of a prognostic cuproptosis-related signature in hepatocellular carcinoma. Biol Direct 2023;18(1):4.
[25] Qin Y, Liu Y, Xiang X, Long X, Chen Z, Huang X, et al. Cuproptosis correlates with immunosuppressive tumor microenvironment based on pan-cancer multiomics and single-cell sequencing analysis. Mol Cancer 2023;22(1):59.
[26] Babady NE, Pang Y-P, Elpeleg O, Isaya G. Cryptic proteolytic activity of dihydrolipoamide dehydrogenase. Proc Natl Acad Sci USA 2007;104(15):6158–63.
[27] Yumnam S, Kang MC, Oh SH, Kwon HC, Kim JC, Jung ES, et al. Downregulation of dihydrolipoyl dehydrogenase by UVA suppresses melanoma progression via triggering oxidative stress and altering energy metabolism. Free Radic Biol Med 2021;162:77–87.
[28] Huang Y, Yin D, Wu L. Identification of cuproptosis-related subtypes and development of a prognostic signature in colorectal cancer. Sci Rep 2022;12(1):17348.
[29] Liu H. Pan-cancer profiles of the cuproptosis gene set. Am J Cancer Res 2022;12(8):4074–81.
[30] Zhang F, Lin J, Feng D, Liang J, Lu Y, Liu Z, et al. Cuprotosis-related signature predicts overall survival in clear cell renal cell carcinoma. Front Cell Dev Biol 2022;10:922995.
[31] Zhang R, Tu J, Liu S. Novel molecular regulators of breast cancer stem cell plasticity and heterogeneity. Semin Cancer Biol 2022;82:11–25.
[32] Chen Y, Jia K, Sun Y, Zhang C, Li Y, Zhang L, et al. Predicting response to immunotherapy in gastric cancer via multi-dimensional analyses of the tumour immune microenvironment. Nat Commun 2022;13(1):4851.
[33] Constantinidou A, Alifieris C, Trafalis DT. Targeting Programmed Cell Death -1 (PD-1) and Ligand (PD-L1): A new era in cancer active immunotherapy. Pharm Ther 2019;194.
[34] Sau S, Petrovici A, Alsaab HO, Bhise K, Iyer AK. PDL-1 Antibody Drug Conjugate for Selective Chemo-Guided Immune Modulation of Cancer. Cancers (Basel) 2019;11(2).
[35] Ngambenjawong C, Gustafson HH, Pun SH. Progress in tumor-associated macrophage (TAM)-targeted therapeutics. Adv Drug Deliv Rev 2017;114:206–21.
[36] Mehla K, Singh PK. Metabolic Regulation of Macrophage Polarization in Cancer. Trends Cancer 2019;5(12):822–34.
[37] Borst J, Ahrends T, Bąbała N, Melief CJM, Kastenmüller W. CD4+ T cell help in cancer immunology and immunotherapy. Nat Rev Immunol 2018;18(10):635–47.
[38] Oh DY, Fong L. Cytotoxic CD4+ T cells in cancer: Expanding the immune effector toolbox. Immunity 2021;54(12):2701–11.
[39] Li X, He Y, Jiang Y, Pan B, Wu J, Zhao X, et al. PathwayTMB: A pathway-based tumor mutational burden analysis method for predicting the clinical outcome of cancer immunotherapy. Mol Ther Nucleic Acids 2023;34:102026.
[40] Wang Q, Li X, Qiu J, He Y, Wu J, Li J, et al. A pathway-based mutation signature to predict the clinical outcomes and response to CTLA-4 inhibitors in melanoma. Comput Struct Biotechnol J 2023;21:2536–46.
[41] Lim S, Liu H, Madeira da Silva L, Arora R, Liu Z, Phillips JB, et al. Immunoregulatory protein B7-H3 reprograms glucose metabolism in cancer cells by ROS-MEDIATED STABILIZATION of HIF1α. Cancer Res 2016;76(8):2231–42.
[42] Chen Q, Jun H, Yang C, Yang F, Xu Y. The pyroptosis-related risk genes APOBEC3D, TNFRSF14, and RAC2 were used to evaluate prognosis and as tumor suppressor genes in breast cancer. J Oncol 2022;2022:3625790.
[43] de Kruijf EM, Sajet A, van Nes JGH, Putter H, Smit VTHBM, Eagle RA, et al. NKG2D ligand tumor expression and association with clinical outcome in early breast cancer patients: an observational study. BMC Cancer 2012;12:24.